STM JOURNALS

Journal of
Automobile Engineering
and Applications

ISSN: 2455-3360
Volume 11, Issue 3, 2024
September—December
DOI Journal: 10.37591/JoAEA

https://journals.stmjournals.com/joaea

Research JoAEA

Energy Harnessing Solution Using a Vertical Axis Wind Turbine Installed on The Automotive Rooftop.

Akshansh Yadav [1,*], Piotr Prusinski [2], Gangesh Singhal [3]

Abstract

The transportation sector plays a major role in greenhouse gas emissions, prompting worldwide initiatives to mitigate its environmental effects. While the shift from internal combustion engines to electric vehicles is growing, it often merely shifts emissions rather than eliminating them, as fossil fuels continue to dominate energy production. A comprehensive solution requires universal access to renewable energy sources like wind, solar, and hydro power, which is currently impractical due to the large scale and low energy density of these plants.This study proposes an innovative solution that advances current approaches by relying on renewable energy, operating independently of weather conditions, being compact and portable, and reducing emissions in real-time by conserving fuel or recharging batteries. This makes it applicable to both electric and fossil-fueled vehicles. The proof-of-concept design features a standard diesel bus equipped with a rooftop turbine box that harnesses wind energy generated during motion, converting it into electrical power. The scaled-down turbine design produces an average net power of 4.8 kW during bus journeys, sufficient to power bus accessories or charge the battery. The study includes computational fluid dynamics (CFD) analysis and the preparation of a 3D model, which was tested in a wind tunnel. The design of inflow guide vanes, turbine blade shape and size, and turbine performance at various inflow velocities and azimuthal positions were investigated, providing practical insights. The wind tunnel study was conducted at the National Wind Tunnel Facility (NWTF), which features a return circuit, continuous closed jet, and atmospheric conditions with interchangeable test sections measuring 3 m × 2.25 m in cross-section and 8.75 m in total length. The wind tunnel achieves a maximum speed of 80 m/s, with a Reynolds number of 5x10^6/m and turbulence below 0.1%. It is equipped with specialized instrumentation, including a 4.64 m diameter, 12-bladed fan powered by a 1000 kW variable-speed DC motor, and a virtual instrumentation-based data acquisition system. The NWTF's primary advantage is its turntable, allowing simulation of wind incidence angles from 0° to 360° in a single test run. Six configurations were evaluated: full-scale device, full-scale device with mesh, full-scale device with fins, scaled bus model, scaled device alone, and scaled device mounted on the bus. Wind tunnel tests were conducted at speeds ranging from 5 to 30 m/s. Experimental results confirmed model stability and the absence of significant vibrations or oscillations during testing. Findings provide insights into the forces, RPM, and stability of the turbine model under various wind conditions, enhancing understanding of aerodynamic behavior and supporting design optimization for automotive structures. This research showcases the versatility and efficacy of the NWTF in aerodynamic testing.

***Author for Correspondence**
Akshansh Yadav
E-mail: akshansh.iitk@gmail.com

[1]Research Scholar, Department of Aerospace, Indian Institute of Technology Kanpur, Uttar Pradesh, India
[2]Research Scholar, Department of Energy, Warsaw University of Technology, Warsaw, Poland
[3]Research Scholar, Department of Energy and Power System, University Liverpool, England

Received Date: July 25, 2024
Accepted Date: August 26, 2024
Published Date: September 21, 2024

Citation: Akshansh Yadav, Piotr Prusinski, Gangesh Singhal. Energy harnessing solution using a vertical axis wind turbine installed on the automotive rooftop. Journal of Automobile Engineering and Applications. 2024; 11(3): 1–21p.

Keywords:

1. Vertical Axis Wind Turbine.
2. Wind Tunnel.
3. Turbulence Model
4. Mesh Convergence Study
5. Azimuthal Angles

INTRODUCTION

The growing number of cars on our roads has significantly increased pollution levels, posing a threat to human health and the environment. Vehicle emissions, including carbon dioxide and other harmful pollutants, contribute to air pollution and climate change. Urgent measures are needed to address this issue, such as promoting electric vehicles, improving public transportation, and enforcing stricter emission standards. This research focuses on efficient transportation solutions in India and Poland, two fast- growing economies grappling with similar problems and working together to find common solutions [1-3].

Table.1. Pollution demographic comparison

	Population (2022)	**Total emissions [GtCO2e] (2019)**	**Emissions per capita [tCO2e]**	**Emissions due transportation [MtCO2e]**
Poland	37,766,327	0.393	10.40	67
India	1,389,637,446	3.274	2.36	292
Ratio	36.8	8.3	0.23	4.4

India ranks as the third-largest global emitter, despite its relatively low per-capita emissions of 2.4 tons of CO2 annually. Its annual emission of 3.3 (2.9 net) gigatons of carbon dioxide equivalent (GtCO2e/a) necessitates urgent action. Nihal et al. [4] mention that India's commitment to achieving net-zero emissions by 2070 at COP26 is significant.

Transportation accounts for 9% of India's carbon emissions, equivalent to 0.292 GtCO2e/a. Comparatively, Poland's total GHG emissions are 0.393 GtCO2e/a, with Poland generating 10.5% of the EU's emissions. Despite efforts towards a greener economy, Nazar et al. [5] suggest that Poland still has the second-highest carbon intensity among EU.

states, with the energy industry and transportation sector contributing significantly to emissions. Transportation significantly impacts the environment (Table 1). While transitioning energy sources and consumption methods in transportation can yield widespread benefits, the complete elimination of fossil fuels remains unlikely soon. The current surge in electro-mobility does not alter the fact that cars primarily rely on power generated by fossil-fired plants.

Converting extensive land into solar and wind farms has limitations. Nevertheless, we can currently diminish our reliance on fossil fuels by employing intelligent energy harvesting and efficient consumption designs that have no negative environmental impact.

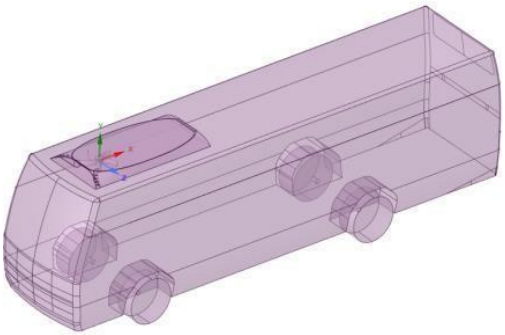

Figure 1. Turbine box mounted on the bus rooftop.

This study proposes a new design of a turbine box that could be attached to the rooftop of buses, coaches, or long-haul vehicles (see Figure. 1). The box embeds an impeller to harness energy as the vehicle moves. This idea is supplementary and does not contradict existing automotive advancements. It can be applied to both combustion engines and electric-driven vehicles.

The research involved conducting a computational fluid dynamics (CFD) analysis, followed by preparing a 3D model for wind tunnel testing. Several studies investigating different factors related to wind turbine integration on buses are summarized below.

Adeyeye et al. suggested that the aerodynamic performance of the bus must remain unaffected after integrating the turbine box on the bus rooftop, as this might impact the bus's performance and add extra weight. Oscar B. Arteaga et al [1]. suggested that attaching aerodynamic deflectors on bus rooftops improves aerodynamics compared to the baseline model. Their research indicated a 3.4% improvement in drag reduction after adding spoilers.

Daniel Garcia-Ribeiro et al. [6] noted that different aerodynamic devices attached to automobiles reduce vortices and affect fuel consumption by reducing drag. Their research showed that vortex generators altered flow behavior on buses, decreasing the drag coefficient by up to 8.63% and fuel consumption by 3.92%. The reference design discussed here was taken into consideration to improve the aerodynamic efficiency and reduce vortices formation.

M. Zahir Hussain et al. [3] proposed a system capable of recharging a vehicle's battery while in motion, utilizing a Vertical Axis Wind Turbine (VAWT) positioned within the vehicle's front grille. This VAWT produced 0.5 kW of energy at speeds of 40–60 km/h. Inspired by this, we designed a five-bladed Savonius VAWT capable of generating 1.2 kW at an average speed of 10 m/s (city bus speed) and up to 4.8 kW at 25 m/s (intercity bus speed) [7-10].

These studies offer valuable insights for optimizing wind turbine integration on buses, improving energy generation, reducing fuel consumption, and minimizing environmental impact.

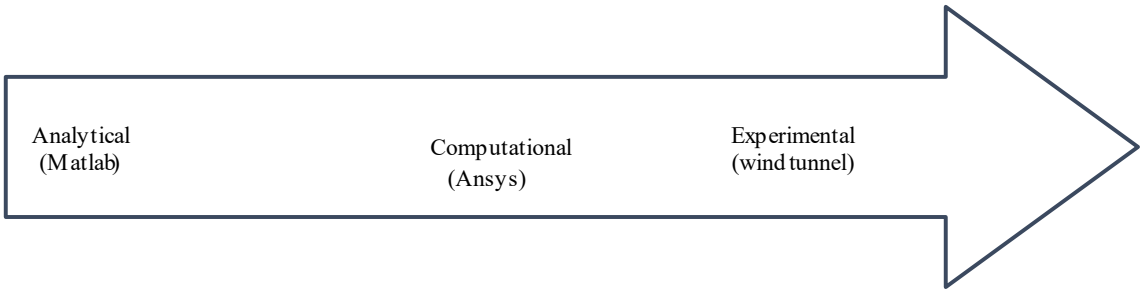

Figure 2. Research paths.

This paper presents the core idea of harnessing wind energy on bus rooftops by installing a turbine that minimally impacts vehicle performance. The turbine box, detailed in Figure. 2, includes a Savonius-based VAWT, known for its drag-based operation. Inflow guide vanes streamline irregular flow. The flow physics analysis investigates bus drag and the additional drag caused by the roof-mounted turbine, offering insights into flow behavior and quantifying the turbine's impact on drag. The study evaluates fuel consumption, power generation, and aerodynamic implications of the turbine unit on bus performance, assessing the turbine's efficiency under real-world conditions. It summarizes the conclusions from the flow physics analysis and power generation calculations, providing a comprehensive overview of the turbine unit's efficiency and performance on a moving bus.

Wind tunnel testing at various velocities using a scaled-down version of the device is essential to assess aerodynamic coefficients and power consumption levels. The actual and scaled dimensions for testing ensure accurate measurements and analysis. By subjecting the scaled-down device to different wind velocities within the wind tunnel, we gather crucial data on its aerodynamic performance, including aerodynamic coefficients and power consumption levels under varying conditions. This empirical data enhances our understanding of the device's performance characteristics, facilitating optimization and validation of theoretical models.

Consequently, wind tunnel testing of the scaled-down device at different velocities plays a pivotal role in the comprehensive analysis of its aerodynamic coefficients and power consumption levels. This information is vital for making informed design decisions,

The test section size of 3m wide 2.25m high and 8.75m long is ideally suited for large scale automotive engineering structures. A sketch of the wind tunnel is shown in Figure 3 & 4. and the important features are listed below:

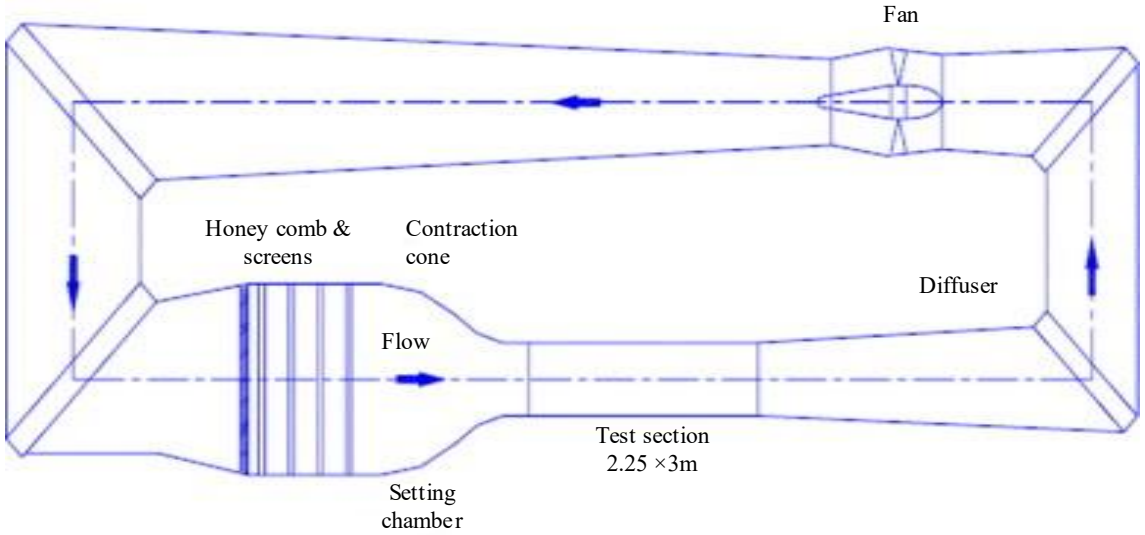

Figure 3. Aerodynamic layout of the wind tunnel facility

The important features of the wind tunnel used in this study:

- Return circuit, continuous closed jet, and atmospheric
- Interchangeable test sections
- Cross-section : 3 m × 2.25 m
- Length : 5.75 m (upstream part) + 3 m (downstream part)
- Contraction ratio : 9:1
- Wind speed: 80 m/sec (Maximum)
- Reynolds number : $5x10^6$/m
- Turbulence level : < 0.1%
- Fan :4.64 m diameter, 12 bladed Motor rating:1000 kW variable speed DC motor, 450 RPM

METHODOLOGY

Computational Design

Figure 4 & 5 The turbine box's outer structure is designed to ensure smooth aerodynamic flow, preventing the formation of wake regions that disrupt flow continuity and create pressure gradients. Inside, a Savonious turbine (drag based) is placed for power generation. Two guide vanes are attached to the turbine inlet to direct airflow toward the turbine blades. The evaluation of this technology employs computational fluid dynamics (CFD) and MATLAB, providing detailed modeling of turbine power, flow behavior, and turbulence effects. CFD simulations accurately capture complex airflow patterns and enable precise data on power generation. The integration of CFD enhances the analysis of airflow dynamics, pressure distribution, and energy conversion, ensuring reliable conclusions about the system's power generation capabilities.

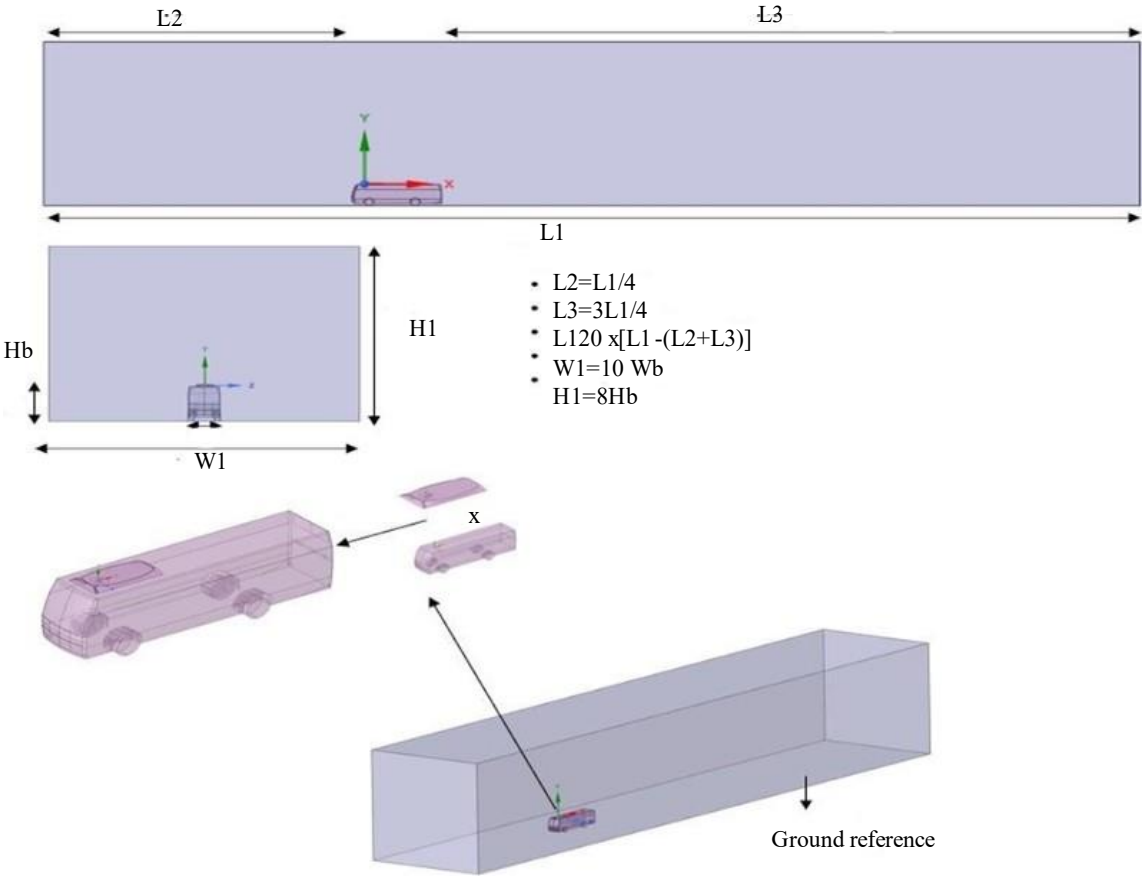

Figure 4. Domain specification for the computational setup.

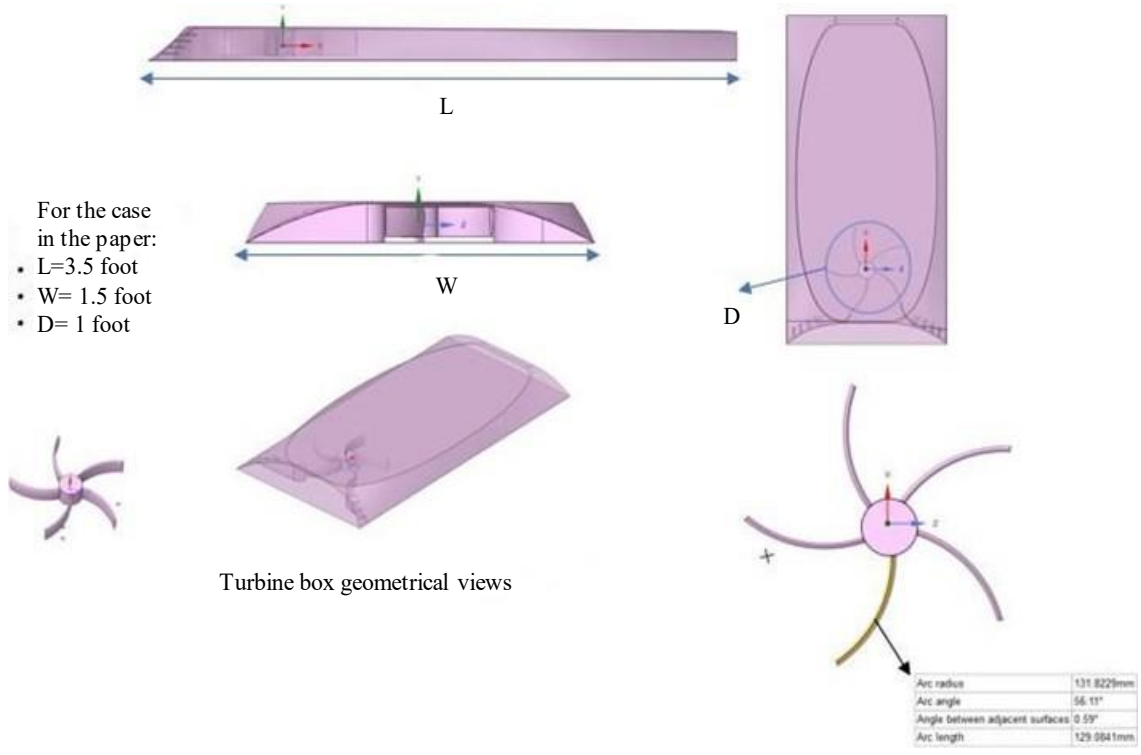

Figure 5. Domain specification for the wind turbine box.

Meshing and Domain Sizing for Accurate CFD Analysis

Figure 6 The computational model accurately represents system geometry by defining airfoil geometry, blade parameters, and domain sizes. Svetlana et. al [11]. gave the reference for the grid convergence study which was taken into consideration while meshing. Computational fluid dynamics (CFD) principles determine the computational domain and mesh elements. The computational domain must be selected in such a manner that the side walls should not interact with the analyzing body while the flow from the inlet. For example, a 20-meter external domain uses 0.4-meter elements, while a 5-meter internal structure employs 0.01-meter elements. Adhering to these guidelines ensures a suitable representation of geometry and domain, enabling precise and reliable CFD analysis for valuable insights into fluid dynamics and system behavior [12].

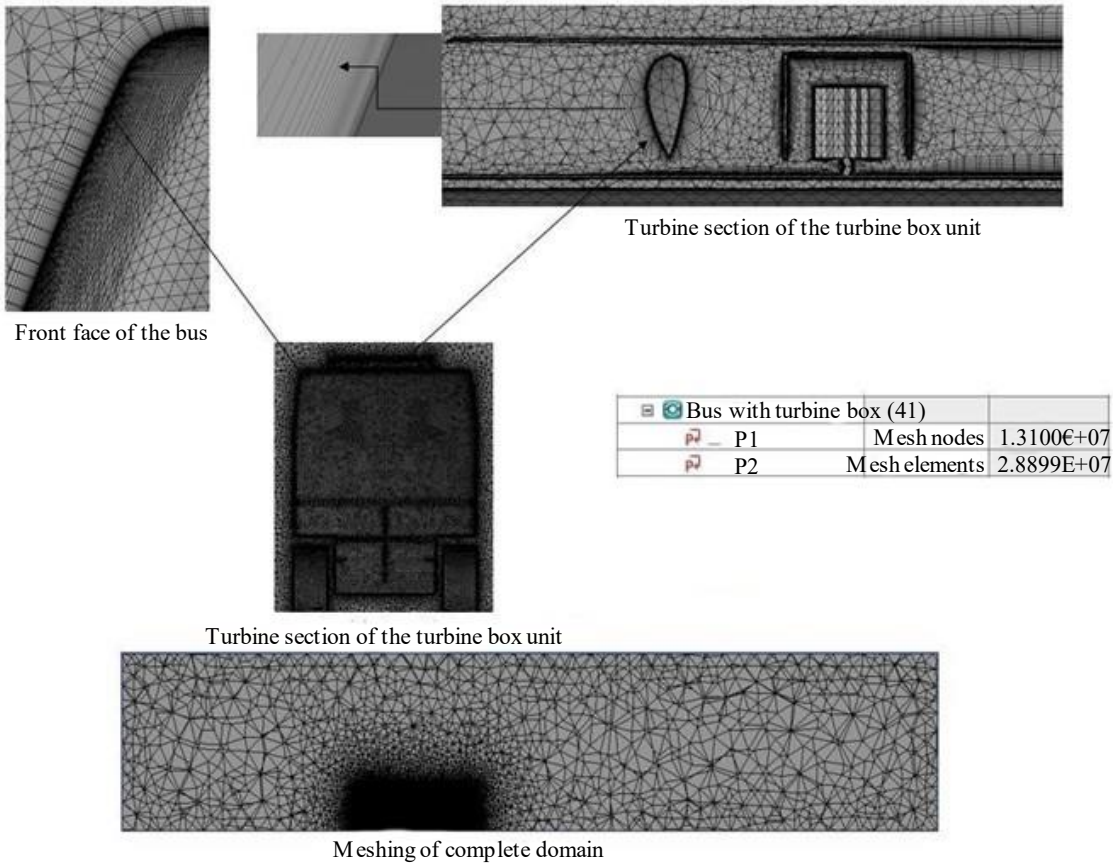

Figure 6. The meshing statistics of the setup.

Reynolds number for the analysis

There are different geometrical setups, but air, the range of velocities and physics are the same in any research, so some common similarity number for all seems to be a good reference point, as a result, the Reynolds number is a good comparison for such kinds of parametric study. The Reynolds number is defined as the ratio of inertial forces to viscous forces and is calculated using the following formula:

$$Re = (\rho * V * L) / \mu \quad (1)$$

where:

- ρ is the density of the air
- V is the velocity of the air
- L is the characteristic length of the bus which is the width of the bus.
- μ is the dynamic viscosity of the air

The Reynolds number varies to a certain range based on its freestream velocities from 12 m/sec to 22 m/sec that we have used in our study. The nature of the flow remains turbulent along the complete velocity range. The range of the Reynolds number used in the study shows a linear progression with the velocity Figure: 7.

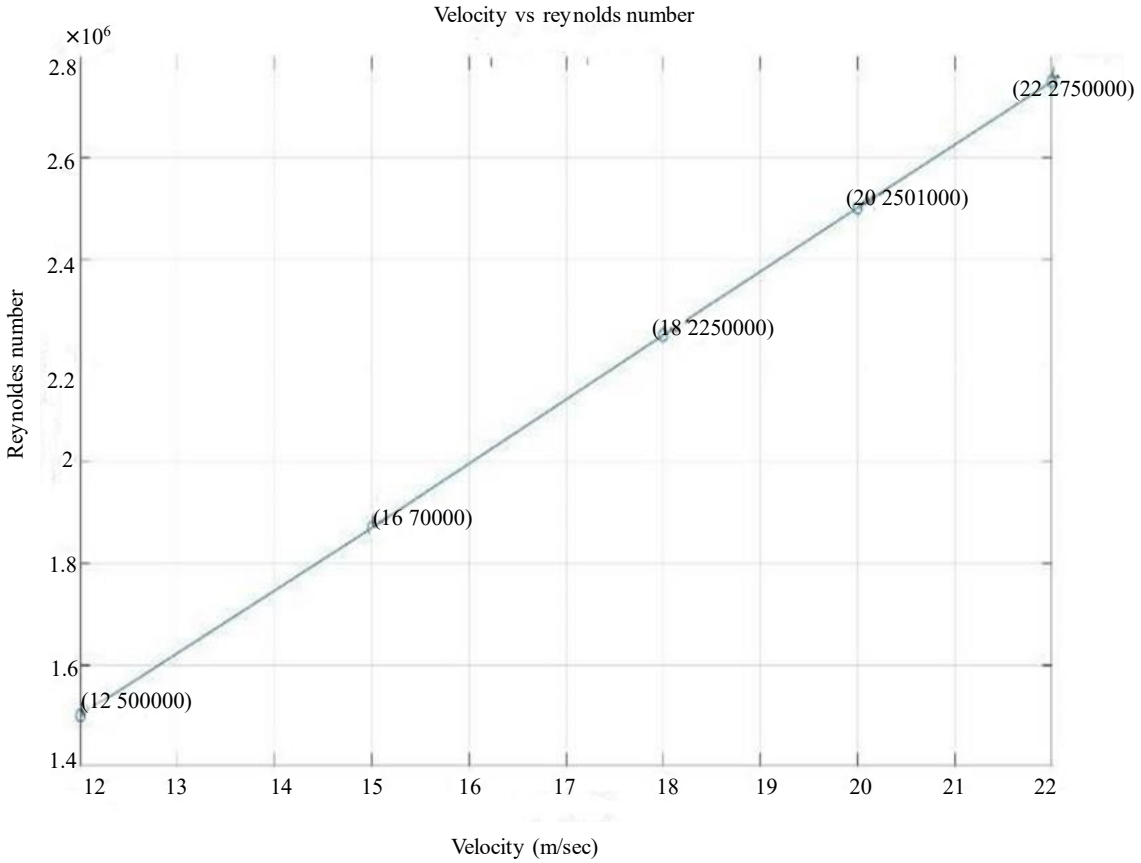

Figure 7. Reynolds Number variation at different freestream velocities

Turbulence Model Selection

Based on a thorough review of relevant research papers, including de Oliveira, Marielle et. al [30], the SST (Shear Stress Transport) k-ω turbulence model is selected as the most suitable choice for analyzing the flow around a bus with a rooftop Vertical Axis Wind Turbine (VAWT). With a calculated Reynolds number falling within the turbulent flow range, the SST k-ω model proves effective in capturing turbulent effects, flow separation, and interactions between the bus and the VAWT. Its comprehensive representation of turbulence characteristics and successful application in similar studies make it a reliable option for obtaining accurate results in this analysis.

In our study, we advance the current approaches in addressing greenhouse gas emissions in the transportation sector by proposing a solution that relies on renewable energy, operates independently of weather conditions, is compact and portable, and reduces emissions in real-time. This solution is applicable to both electric and fossil-fueled vehicles, featuring a diesel bus equipped with a rooftop turbine that harnesses wind energy generated during motion, converting it into electrical power. The designed turbine produces the power of 4.3kW at a freestream velocity of 25m/sec and 5.6kW at the freestream velocity of 30m/sec which is validated computationally and experimentally.

The design and performance of our turbine were analyzed using computational fluid dynamics (CFD) and tested in a wind tunnel. Several studies have provided significant insights into bus aerodynamics and wind turbine performance. Han, Lee, and Kim (2018) investigated bus aerodynamics using different

turbulence models to understand their impact on predictions (Han et al., 2018). Another study by Lee, Cho, and Park (2019) utilized the SST k-ω turbulence model to analyze bus airflow, evaluating its aerodynamic performance Alonso-Estébanez, A., Del Coz Díaz et al. [36]. Yoon, Park, and Kang (2017) conducted a numerical study of wind effects on bus aerodynamics using a turbulence model (Yoon et al., 2017) [13-18].

Additionally, research on wind turbine performance has also informed our approach. explored turbulent airflow over vertical-axis wind turbine blades and its impact [19-22].

Naik and Ransing et. al [39], evaluated horizontal-axis wind turbine performance using the SST k-ω turbulence model to enhance efficiency and power generation. Examined the effect of turbulence models on the aerodynamic analysis of wind turbines, emphasizing the necessity of the SST k-ω equation for better design and performance optimization et al., [23-28], which we also used in our study as a prominent Reynolds-Averaged Navier-Stokes (RANS) equation

Our findings provide insights into the forces, RPM, and stability of the turbine model under various wind conditions, supporting design optimization for automotive structures and showcasing the NWTF's versatility in aerodynamic testing.

The selection of the SST k-ω turbulence model for our research holds significant value, particularly in the context of analyzing a moving bus with a rooftop turbine box at operational speeds below 60 km/h. The SST k-ω model's ability to accurately predict complex flow behaviors, such as boundary layer dynamics, separation, and reattachment, aligns perfectly with our study's focus. By leveraging this model, we aim to gain precise insights into the aerodynamic interactions between the bus, turbine box, and surrounding airflow. Its well-established track record in accurately simulating low- speed flows, coupled with its adaptability to challenging configurations, ensures that our research yields comprehensive and reliable results, shedding light on the intricate aerodynamic nuances of our innovative bus-turbine system [33].

Mesh convergence study

During the analysis of the mesh for the device we tried finding the ideal size of the mesh domain that would further not result in the variation of the results down the line and for that purpose we had a mesh convergence study in which an effort was made to find the correct element sizing after which there was no further variation in the results. Also, an effort was made to put the Y+ value under control. For the skewness ratio, the acceptable value must be closer to 0 & a typical range for the aspect ratio is 1 to 10, with lower values indicating more regular elements [34].

Table 2. Mesh convergence study

Mesh type	No of elements	Outerdo main size	Innerdo main size	No of inf. layers	Cd	Y+Max	Skewness (maximum)	Aspect ratio (maximum)
tetrahedron	7 million	0.65	0.03	0	0.448	18.24	0.8	12.50
tetrahedron	8 million	0.65	0.02	0	0.449	10.08	0.75	16.24
tetrahedron	10 million	0.65	0.02	20	0.452	7.43	0.38	10.55
tetrahedron	12 million	0.65	0.02	40	0.456	1.2	0.18	10

To verify the mesh convergence study, we have increased the velocity of freestream air from 12m/sec to 15m/sec, there was no change in the aerodynamic coefficient's despite of change in the aerodynamic forces. This shows that the mesh is even tailored Since the mesh refinement and velocity change as mentioned in (table.2) doesn't affect the aerodynamic coefficients, the mesh is said to be converged [35].

RESULTS AND DISCUSSION

Figure 8 Here in this computational setup, we are trying to see a comparison in the flow pattern at the inlet when the guide vanes are present and without the guide vanes. This comparison is basically to show how the attachment of the guide vanes helps in the alignment of the airflow in a laminar pattern which does not happen in the configuration where guide vanes are absent, there the flow is predominantly turbulent in its nature [36].

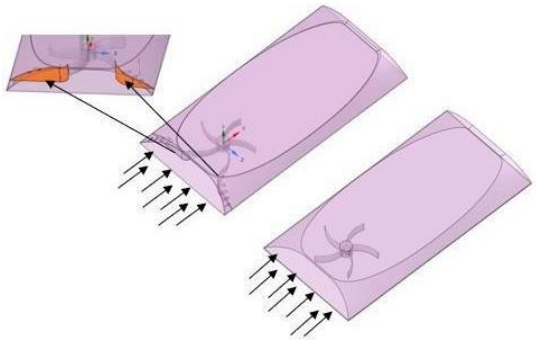

Figure 8. Turbine box with guide vane (left) and turbine box without guide vane (right)

Due to the streamlined flow, the impact force on the blades gts increased, and due to this the angular velocity and the power output are enhanced.

In Figure., 9 & 10 through the velocity and vector plot comparison, it is clearly shown that the use of guide vane has resulted in the regularization of the flow at the inlet and the velocity at the inlet increases because of which the impact force at the turbine blades gets increased and the power output is more [37].

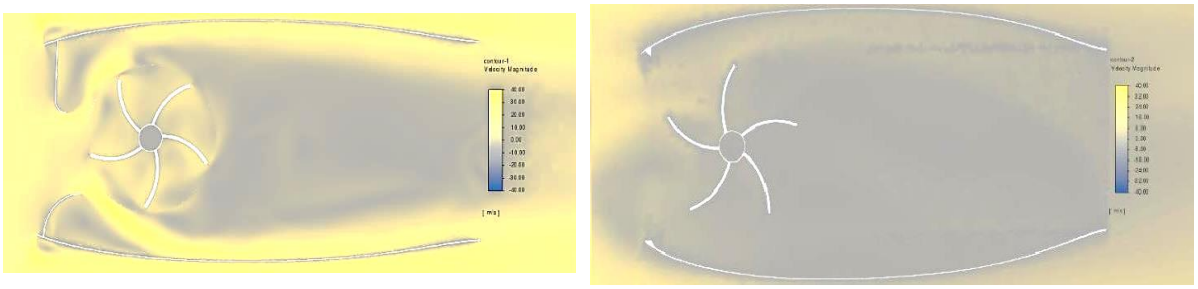

Figure9. Top View of the flow passing the device while bus cruise with (top) or no guide vanes (bottom).

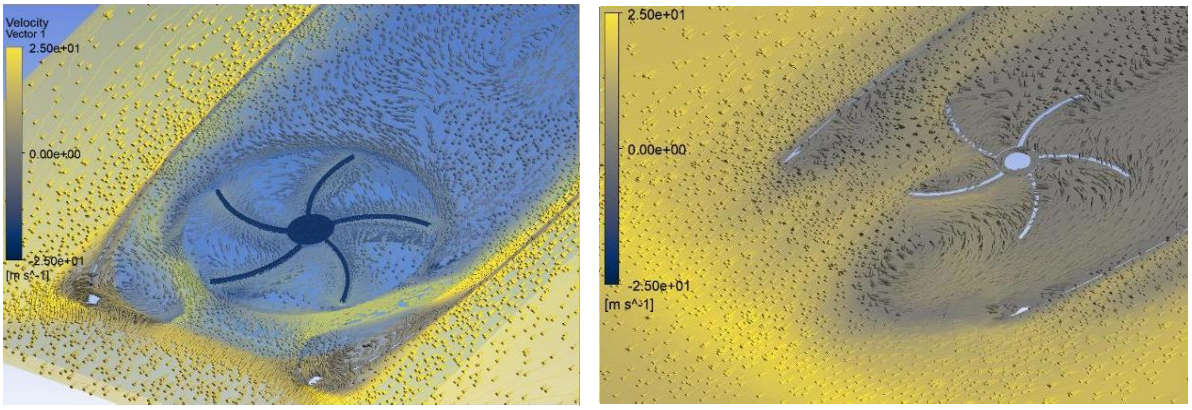

Figure 10. Vector flow visualization of the flow passing the device while the bus cruise with (top) or no guide vanes (bottom).

The computational analysis reveals that guide vanes effectively streamline the flow, resulting in increased power delivery by the turbine. Laminar flow is achieved, reducing vortex formation, and minimizing the wake region behind the turbine [38]. The figure clearly demonstrates that the presence of guide vanes reduces negative pressure regions (as shown in Fig. 11) compared to the absence of guide vanes in the turbine box.

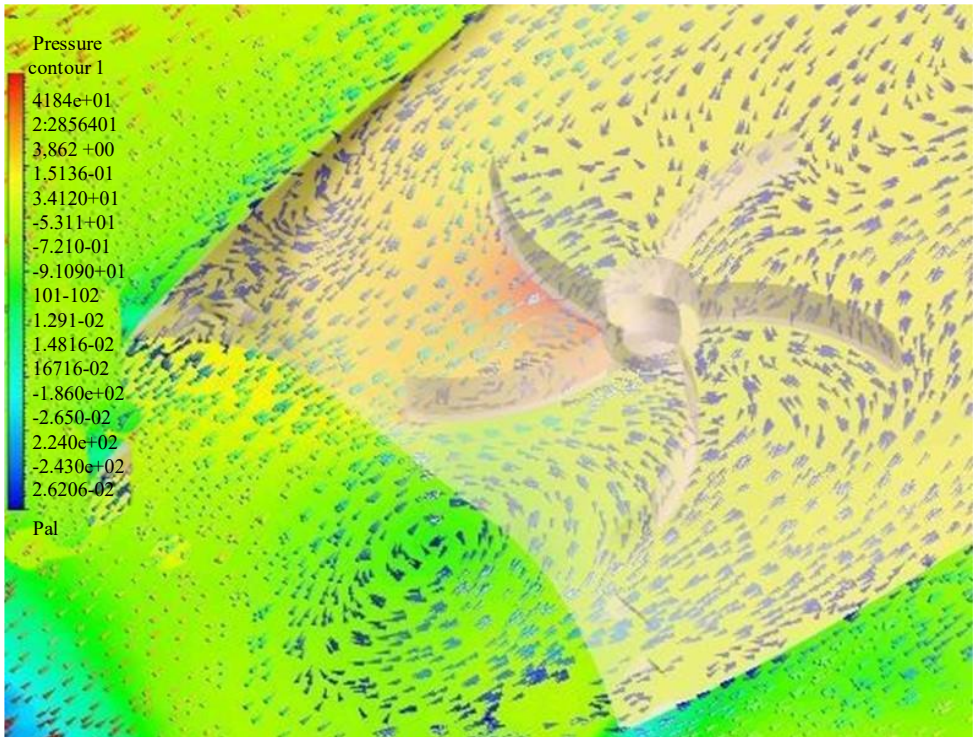

Figure 11. Negative pressure regions without guide vanes.

Table 3. Performance coefficients for guide vanes attachment.

	Cl	Cd	Cm	Cp
Wind panel (with GV)	0.052	0.018	-0.005	0.75
Wind panel (without GV)	0.057	0.024	-0.0032	0.58

The above Table 3, shows the aerodynamic coefficients of the external body with and without the guide vanes. This study was done without the bus, and the purpose of this study is to have a distinguished result with and without the guide vanes and to show the change in the parameters with the guide units. This study helps us to conclude that the external drag of the body gets reduced [39].

Power Calculations with the guiding vanes attachment on the turbine

A guiding vane nozzle, or converging nozzle, accelerates fluid by reducing pressure. Placed before a wind turbine, it funnels and speeds up the incoming air, boosting power production. The nozzle narrows, causing air velocity to rise through the conservation of mass and energy. This high-speed air energizes the turbine blades, increasing power output. In conclusion, a guiding vane nozzle ahead of a wind turbine enhances air velocity, thus elevating power generation through heightened kinetic energy [40].

Mathematical Calculation to Prove That Power Produced by The Turbine with Guiding Vane Is More Than Without Vanes

Without guiding vanes, the wind flows directly onto the turbine blades, causing the blades to rotate and turn the rotor. However, some of the wind energy is lost due to turbulence and wake effects behind

the blades. Now, let's add guiding vanes to the turbine. The guiding vanes are placed in front of the turbine blades and direct the wind onto the blades at an optimal angle, reducing turbulence and wake effects. This allows the blades to extract more energy from the wind, resulting in higher power output. The power produced by a wind turbine is given by the following formula:

$$P = (1/2) \times rho \times A \times Cp \times V^3 \quad (2)$$

where:

- P = power produced by the wind turbine (in watts) rho = air density (in kg/m^3)
- A = area swept by the turbine blades (in m^2)
- Cp = power coefficient (dimensionless, depends on the design of the turbine) V = wind speed (in m/s)

Assuming the same wind speed and blade design, we can compare the power output of a wind turbine with and without guide vanes. Let us assume that the area swept by the blades is 0.62 and the air density is 1.225 kg/m^3.

Comparing the two equations, we can see that P2 is greater than P1. Therefore, the power produced by the turbine with guiding vanes is more than without vanes, assuming the same wind speed and blade design.

This calculation is based on several assumptions and simplifications, so the actual increase in power output due to guiding vanes may vary depending on the specific design and installation of the wind turbine.

Table 4. Power output comparison with and without guide vane.

Velocity (m/sec)	Power without a guide vane (watts)	Power with guide vane (watts)
5	28.125	38.125
10	225	305
15	743.2345	1026
20	1762	2357.234
25	3442	4748

Computational and comparative study

To study the fluid flow and the power outputs from the installed turbine by the guide vanes, we have used computational and analytical approaches. However, it's important to consider their assumptions and limitations and verify results against experiments or analytical solutions when possible. In this case study, we compared analytical and computational approaches to emphasize the benefits of using guided vanes in the turbine box. Theoretical analysis revealed that adding guided vanes increases the theoretical power extracted from the turbine by generating an additional resultant force through laminar flow. Computational analysis with flow visualization techniques confirmed this enhancement at different velocities. The consistent trend of increasing power with guide vanes supports their implementation at the turbine box inlet. Figure. 7 displays the power generated by the turbine with and without guide vanes, compared to CFD analysis. Mathematical modeling provides a trendline, while computational analysis delivers a more accurate and optimized solution.

In the below Figure 12, the graph is plotted to show the change in the power output due to guide vanes, where the above-mentioned approaches are plotted together.

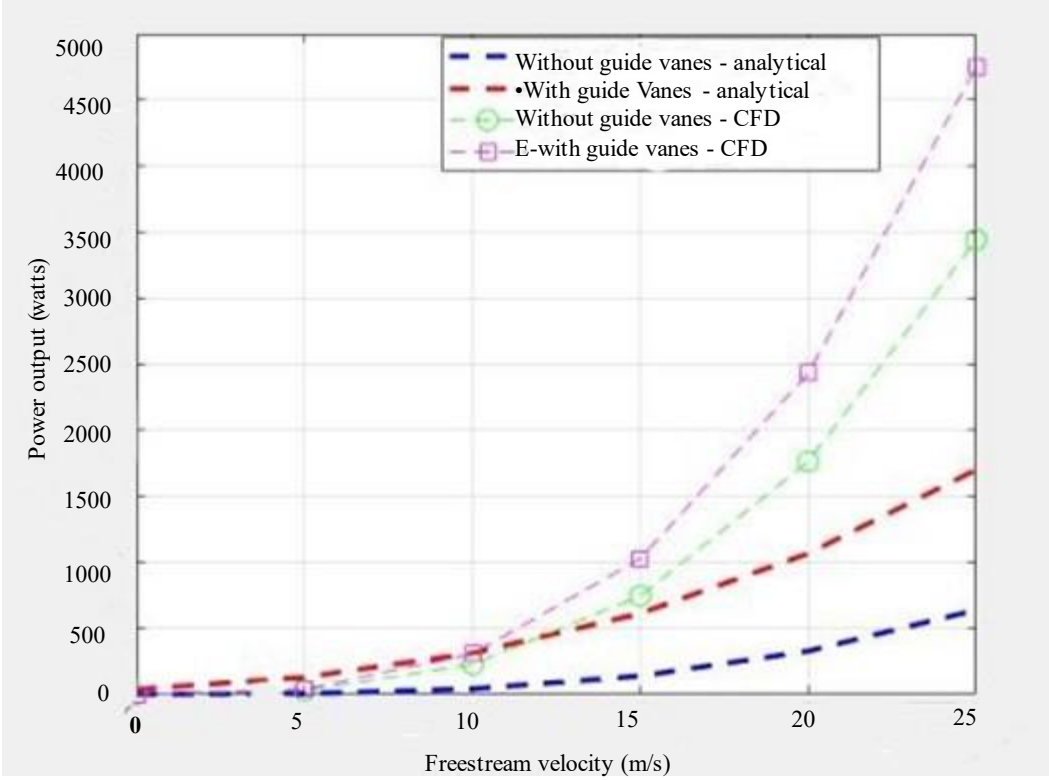

Figure 12. Effect of the guide vane on turbine power output.

To determine the power generated by a single blade of a 5-bladed impeller at different positions, follow these steps:

- Define the blade's shape and characteristics.
- Specify the wind speed and turbine rotation speed.
- Calculate the local velocity and angle of attack for each blade section.
- Determine the lift and drag coefficients for each blade section using XFOIL or similar techniques.
- Compute the lift and drag forces for each blade section.
- Calculate the tangential and normal forces for each blade section.
- Determine the power generated by each blade section.
- Sum up the power generated by each blade section at various azimuthal locations.
- Perform a transient CFD analysis to observe how the power changes with different azimuthal positions.

The power produced by a turbine single blade at different azimuthal locations can be calculated using the following formula:

$$P(\theta) = (1/2) * \rho * A * V^3 * Cp(\theta) \quad (3)$$

Where:

- P = Power produced by the turbine blade ρ = Air density
- A = Area swept by the turbine blade V = Wind speed
- Cp(θ) = Coefficient of performance of the turbine blade at a particular azimuthal angle θ

Table 5 The coefficient of power of the blade element can be calculated using the lift and drag coefficients of the blade element:

$$Cp = (Cl * \cos(phi) - Cd * \sin(phi)) * \sin(alpha) \quad (4)$$

where:

- Cl = lift coefficient Cd = drag coefficient
- phi = angle between the blade element chord and the relative wind direction alpha = angle of attack of the blade element

The values of lift and drag coefficients can be determined from aerodynamic tables or using computational fluid dynamics (CFD) simulations.

So, to evaluate the power consumption evaluation and aerodynamic coefficient analysis, MATLAB is used which is shown in Table 4, and all the power coefficient curves were obtained at different azimuths of the single blade. The single blades turbine was modeled using MATLAB and the power consumption gets plotted at all the azimuths with aerodynamic coefficients.

The coefficient of performance (Cp) of the turbine blade depends on several factors, including the blade design, the rotational speed, and the angle of attack. It can be determined experimentally or through computational simulations.

In the above formula, θ represents the azimuthal angle, which determines the orientation of the blade with respect to the incoming wind direction.

Table.5. Aerodynamic coefficients at different azimuthal angles.

Azimuthal angle	Cl	Cd
0	0.000	0.012
10	0.240	0.014
20	0.470	0.017
30	0.670	0.021
40	0.820	0.027
50	0.910	0.035
60	0.940	0.044
70	0.910	0.056
80	0.820	0.068
90	0.670	0.081
100	0.470	0.094
110	0.240	0.105
120	0.000	0.114
130	-0.240	0.120
140	-0.470	0.122
150	-0.670	0.120
160	-0.820	0.114
170	-0.910	0.105
180	-0.940	0.094
190	-0.910	0.081
200	-0.820	0.068
210	-0.670	0.056
220	-0.470	0.044
230	-0.240	0.035
240	0.000	0.027
250	0.240	0.021
260	0.470	0.017
270	0.670	0.014

280	0.820	0.012
290	0.910	0.012
300	0.940	0.012
310	0.910	0.012
320	0.820	0.014
330	0.670	0.017
340	0.470	0.021
350	0.240	0.027
360	0.000	0.035

Figure 13 & 14 Below is the graph for the power produced by the turbine blade at different azimuths. Below is the power coefficient graph at different azimuths using the MATLAB solver. Now through the thing, curve plots it's clear that in between the azimuths of 30 to 120 degrees, the power produced is positive, and then the turbine will produce less or negative power. The net power through the NACA0015 airfoil gets positive.

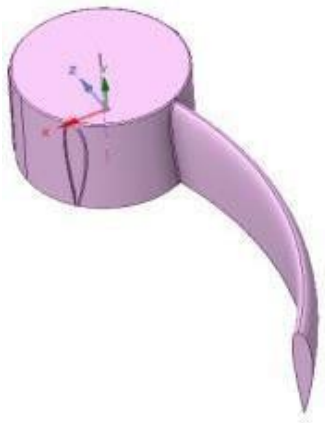

Figure 13. Single-blade turbine

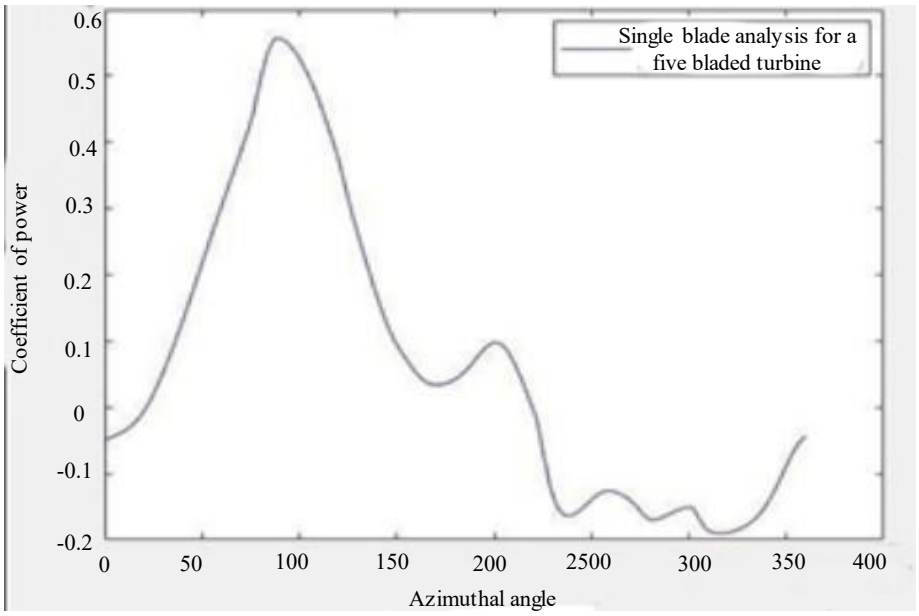

Figure 14. Power from the blade at different azimuths

A vertical axis wind turbine (VAWT) relies on blade chord length and advance ratio for optimal performance. The chord length affects lift and drag, while the advance ratio impacts efficiency and stall conditions. The ideal chord length and advance ratio depend on wind speed, blade material, and turbine size. Computational fluid dynamics and wind tunnel testing determine the best blade design. Guide vanes control airflow and their size, orientation, and curvature influence the entering air's angle and velocity. Achieving laminar flow before the turbine blade is crucial, and curved or angled vanes are effective. CFD analysis examines different guide vane parameters and twist angles' impact on turbine performance [38].

Experimental Setup and prototype testing in Wind Tunnel:
The following configurations were tested in the wind tunnel:

a. *Configuration 1:* Full-scale device.
b. *Configuration 2:* Full-scale device with mesh.
c. *Configuration 3*: Full-scale device with fins.
d. *Configuration 4:* Scaled bus model.
e. *Configuration 5*: Scaled device alone.
f. *Configuration 6:* Scaled device mounted on bus.

Figure 15. Configuration 1: full-scale device.

Figure 16. Configuration 5: scaled device alone.

All the six configurations were tested where the turbine has been operated at different freestream velocities and the power from the turbine and the drag of the body has been computed at different conditions, from the suggested series of tests the drag computed for the complete assembly of the bus with device installed on the roof-top does not affect the aerodynamic drag as the frontal surface area remains the same as before without the device installed over the bus rooftop. The results discussed in the table below suggest a coherence with the simulated data on CFD.

Table 6. Forces on the full-scale device with fins

Velocity (m/s)	Drag Force (N)	Side Force (N)	Lift Force (N)	Turbine Power (W)	RPM
10	4.73	-0.02	19.84	266	180
15	10.3	0.02	31.95	940	270
20	18	0.01	43.84	2086	420
25	27.21	0.15	21.41	4300	540
30	38.37	0.13	36.97	5600	660

From Table 6.a, when the values of the turbine power were compared between CFD and Wind tunnel results, the results from CFD over predicts the turbine power by 10%.

Table 7. Forces on the bus model without the device on rooftop

Velocity (m/s)	Drag force (N)	Side force (N)	Lift force (N)
5	6.26	-0.31	17.12
10	23.91	-0.26	30.558
15	54.26	-1.3	45.95
18	75.78	-0.8	35.36

Table 8. Forces on the scaled device mounted on the bus model

Velocity (m/s)	Drag force (N)	Side force (N)	Lift force (N)
5	7.41	-0.38	9.71
10	25.09	-0.14	26.2
15	56.31	-1.54	41.25
18	79.8	-0.91	13.08

As marked in the Figures 17 and 18, it was observed that due to the additional increment in the frontal surface area due to the roof top model mounting, the drag penalty does not increase much because the increase in the frontal surface area is 5%, as a result the penalty on the drag is marginal.

From the above Tables 7 and Table 8, its inferred that the drag increment after the device mounting has hardly increased by 5.26% at 18 m/s.

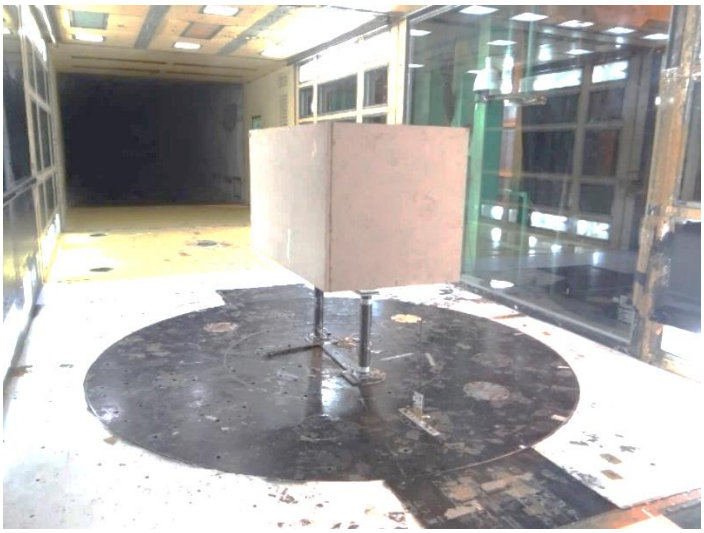

Figure 17. Scaled bus wind tunnel model.

Figure 18. Scaled bus & device wind tunnel model.

Table 9. Results showing the amount of power consumption due to the turbine box installation over the bus vs the power generation capacity of the turbine at different velocities.

Bus velocity (m/sec)	`Power due to the turbine installed over the bus rooftop (in watts)	Power Loss [A] (drag force) due to the attachment on the bus (in watts)	Power Loss [B] (drag force) without the attachment on the bus (in watts)	Difference (A-B) watts
5	40	38	32	6
10	266	251	242	9
15	940	845	825	20
20	2086	1640	1580	60
25	4300	2550	2480	70

In the Table.9, the relation has been developed to show the difference in the aerodynamic power requirement due to the drag increment after the attachment of the turbine box over the bus rooftop and comparing the drag penalty with the aerodynamic power that is generated from the turbine at different freestream velocities.

- The wind tunnel study, measured forces, RPM, and observed model stability through video recording.
- The turbine box model demonstrated stability throughout the tested wind speed range of 5to 30 m/s across all six configurations.
- No significant vibrations or oscillations were detected, affirming the model's robustness and structural integrity.

The configurations explained in Table 10, show that the amount of power generation by the turbine is always possibly more when calculated and compared with the drag power consumption due to the bus and the bus with the device. Also, the addition of the device over the bus doesn’t bring any extra drag on its profile because of which the power consumption due to drag doesn’t get affected a lot after the addition of the device over the bus.

As the size of the bus device is relatively smaller it won't be contributing much towards the addition of the weight due to its installation and won't be adding up the power consumption levels due to the drag. By evaluating the mass properties as shown in Figure 19, of the device used we have found out that the mass of the device is approximately 4Kgs.

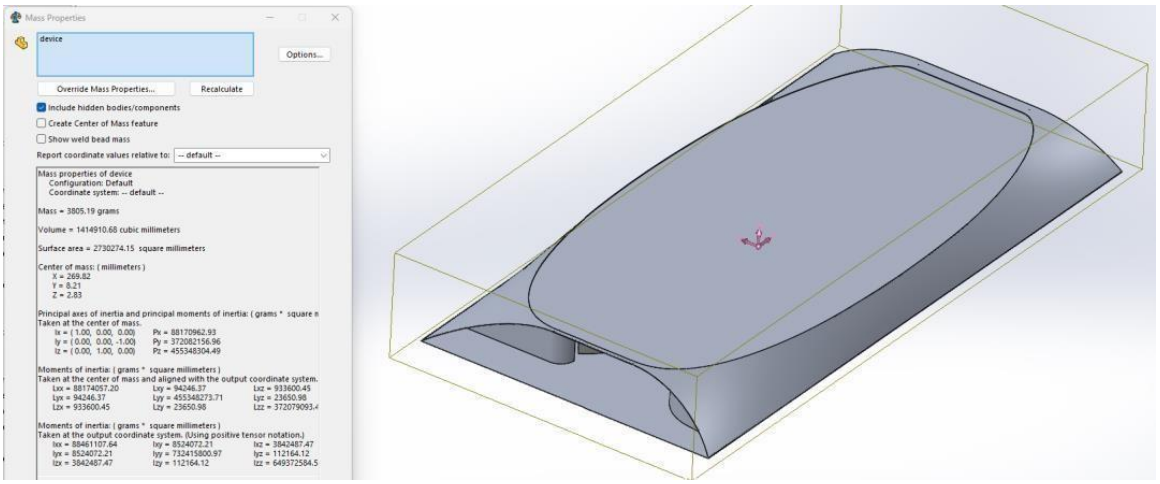

Figure 19. Mass properties evaluation of the turbine box

Table 10. Aerodynamic coefficients with and without the device on the bus rooftop

Device on the bus rooftop	Without device on the bus rooftop
Coefficient of Lift	Coefficient of Lift
0.0152	-0.012
Coefficient of Drag	Coefficient of Drag
0.0745	0.052

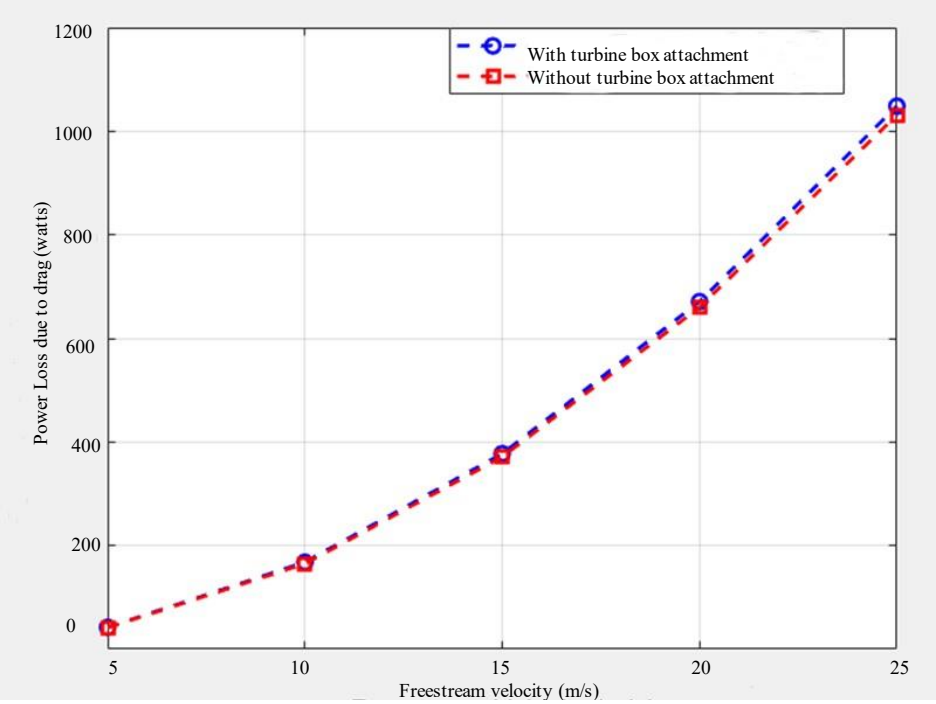

Figure 20. Graphical representation to show the change in the power consumption levels (due to drag force) on the bus when the turbine box is present and not present.

Figure 20 In summary, our research indicates that the turbine on the bus generates more power than it consumes due to drag, making the setup effective in harnessing energy. The scaled-down model used in our study produces around 4.8 kW at a velocity of 25 m/sec (85 km/h). This serves as a reference for scaling up the turbine or using multiple small turbines for increased power output. Optimizing airflow with guiding vanes improves performance without significantly impacting fuel consumption. In

conclusion, attaching a turbine box with guiding vanes to a bus can effectively address power shortages in transportation. Future studies should explore long-term environmental effects and the feasibility of large-scale implementation. Mobile et. al. also mentions the wind farm for increasing the power output through VAWT. The reason behind not using a bigger turbine was that such concepts of a wind turbine cluster can only be used in a wind farm, but it can't be used over the vehicle rooftop. But the idea can be taken as a reference to create large power.

CONCLUSION

To explain the results from Table 10, the power generated by the turbine box is evaluated at a wide range of the bus velocities. Then to evaluate the efficiency of the turbine box installation over the bus rooftop, the power loss due to the drag force is being estimated in the cases when the turbine box is installed over the rooftop with the power consumption when the turbine box is not installed over it. After the comparative study, it is found that the difference in the power consumption (due to drag) after mounting it on the bus rooftop is small. The primary reason behind this is that the frontal surface area of the bus does not change after the installation over the bus rooftop, as the turbine box dimension is (3.5foot x 1.5foot x 0.7foot) which hardly increases the frontal surface area. As the size of the bus is comparatively large when it’s compared with the turbine box the front surface area doesn’t get affected due to this addition on its rooftop.

The study compares turbine power output with the power loss caused by drag from the turbine box on the bus. Power output relies on extracting energy and rpm due to bus velocity, while power loss is due to resistance from the turbine box.

Future Work

Certainly, to extract the mechanical output from the turbine this aerodynamic power generated by the turbine needs to be coupled with the alternator and then extract that power and store it in terms of energy into the battery. The effort requires a physical selection of the motor/alternator of desired torque and then design a gearbox according to the required coupling. The future plan is to do physical testing and integrate the gearbox assembly with the turbine and then utilize this setup to store energy.

The ongoing sturdy discussed in the paper gives us a thorough background about the aerodynamic power that is generated from the turbine and shows us the path line to integrate the turbine with the alternator to validate our study further by continuing the testing after the complete assembly integration and evaluate the energy stored in the battery.

REFERENCES

1. Al-Sharify T, Alanssari AI, Al-Sharify MT, Ali IR. Theoretical physics to improve radio frequency in 5 generation. InIOP Conference Series: Materials Science and Engineering 2020 Jun 1 (Vol. 870, No. 1, p. 012021). IOP Publishing.
2. Garcia-Ribeiro D, Bravo-Mosquera PD, Ayala-Zuluaga JA, Martinez-Castañeda DF, Valbuena-Aguilera JS, Cerón-Muñoz HD, Vaca-Rios JJ. Drag reduction of a commercial bus with add-on aerodynamic devices. Proc Inst Mech Eng Part D J Automob Eng. 2023 Jun;237(7):1623-36.
3. Hussain MZ, Anbalagan R, Jayabalakrishnan D, Muruga DN, Prabhahar M, Bhaskar K, Sendilvelan S. Charging of car battery in electric vehicle by using wind energy. Mater Today Proc. 2021 Jan 1;45:5873-7.
4. Gupta R, Malik D, Sankhe S, Unni N. Decarbonising India: Charting a pathway for sustainable growth. McKinsey Sustainability, October. 2022. Ava From : https://www.mckinsey.com/capabilities/sustainability/our-insights/decarbonising-india-charting-a-pathway-for-sustainable-growth
5. ERBACH G. Climate action in Poland: Latest state of play. Ava from: https://policycommons.net/artifacts/1861051/climate-action-in-poland/2609393/
6. Zamre P, Lutz T. CFD analysis of a Darrieus vertical-axis wind turbine installation on the rooftop of buildings under turbulent inflow conditions. Wind Energy Sci Discuss. 2021 Oct 11;2021:1-27.

7. Silva JE, Danao LA. VAWT cluster parameter study on overall cluster performance, Part II: oblique angles and direction of rotation. In: Proceedings of the World Congress on Engineering 2018. Vol. 2.
8. Hassanpour M, Azadani LN. Aerodynamic optimization of the configuration of a pair of vertical axis wind turbines. Energy Convers Manage. 2021 Jun 15;238:114069.
9. Hassanpour M, Azadani LN. Aerodynamic optimization of the configuration of a pair of vertical axis wind turbines. Energy Convers Manage. 2021 Jun 15;238:114069.
10. Haurissa J, Soenoko R. Analysis of cross flow turbine performance with guide passage gate vane (GG) at runner turbine by using a triangle velocity method. Int J Mech Prod Eng Res Dev. 2020;10(3):10743-54.
11. Qasim A, Usubamatov R, Zain Z. Analysis of impeller type wind turbine. IIUM Eng J. 2011 Dec 20;12(3). Ava from: https://journals.iium.edu.my/ejournal/index.php/iiumej/article/view/153
12. Adeyeye KA, Ijumba N, Colton J. The effect of the number of blades on the efficiency of a wind turbine. In: IOP Conference Series: Earth and Environmental Science. 2021 Jun 1;801(1):012020. IOP Publishing.
13. Elia A, Taylor M, Gallachóir BÓ, Rogan F. Wind turbine cost reduction: a detailed bottom-up analysis of innovation drivers. Energy Policy. 2020 Dec;147:111912.
14. Jadhav CR, Chorage RP. Modification in commercial bus model to overcome aerodynamic drag effect by using CFD analysis. Results Eng. 2020 Jun;6:100091.
15. Alomar OR, Abd HM, Salih MM, Ali FA. Performance analysis of Pelton turbine under different operating conditions: an experimental study. Ain Shams Eng J. 2022 Jun;13(4):101684.
16. Gao L, Yang S, Abraham A, Hong J. Effects of inflow turbulence on structural response of wind turbine blades. J Wind Eng Ind Aerodyn. Ava from: https://www.sciencedirect.com/science/article/abs/pii/S0167610520300477
17. Ngoc DM, Techato K, Niem LD, Yen NT, Dat NV, Luengchavanon M. A novel 10 kW vertical axis wind tree design: economic feasibility assessment. Sustainability. 2021 Nov 17;13(22):12720.
18. BRIEFING: EU progress on climate action - How are the Member States doing?. Climate action in Poland: Latest state of play. Available from: https://www.europarl.europa.eu/RegData/etudes/BRIE/2021/698766/EPRS_BRI%282021%2969 8766_EN.pdf
19. Muthuvel A, Murthi MK, Sachin NP, Koshy VM, Sakthi S, Selvakumar E. Aerodynamic exterior body design of bus. Int J Sci Eng Res. 2013 Jul;4(7):2453-7.
20. Menter FR. Two-equation eddy-viscosity turbulence models for engineering applications. AIAA J. 1994 Aug;32(8):1598-605.
21. Menter F. Zonal two equation kw turbulence models for aerodynamic flows. In23rd fluid dynamics, plasmadynamics, and lasers conference 1993 Jul 6 (p. 2906). Ava From: https://arc.aiaa.org/doi/abs/10.2514/6.1993-2906
22. Menter FR. Improved two-equation k-omega turbulence models for aerodynamic flows. 1992 Oct 1. Ava From: https://ntrs.nasa.gov/citations/19930013620
23. Menter F. Zonal two equation kw turbulence models for aerodynamic flows. In23rd fluid dynamics, plasmadynamics, and lasers conference 1993 Jul 6 (p. 2906). Ava from: https://arc.aiaa.org/doi/abs/10.2514/6.1993-2906
24. Myeong HG. Hybrid RANS/LES method for turbulent channel flow. Trans Korean Soc Mech Eng B. 2002;26:1088-94. doi:10.3795/KSME-B.2002.26.8.1088.
25. Munson BR, Rothmayer AP, Okiishi TH. Fundamentals of fluid mechanics. Wiley Global Education; 2012 Apr 23. Ava from: https://students.aiu.edu/submissions/profiles/resources/onlineBook/L5g8S6_Fundamentals_of_Fluid_Mechanics-_7.pdf
26. Tennekes H, Lumley JL. A First Course in Turbulence. A First Course in Turbulence. 1972;30:2515.
27. Bouhelal A, Smaïli A, Guerri O, Masson C. Numerical investigation of turbulent flow around a recent horizontal axis wind turbine using low and high Reynolds models. J Appl Fluid Mech. 2018;11:151-64. doi:10.29252/jafm.11.01.28074.

28. de Oliveira, Marielle & Puraca, Rodolfo & Carmo, Bruno. (2022). Assessment of turbulence models for the simulation of the flow through a megawatt scale wind turbine rotor. 10.26678/ABCM.EPTT2022.EPT22-0008.Ava from: https://www.researchgate.net/publication/364894065_Assessment_of_turbulence_models_for_the_simulation_of_the_flow_through_a_megawatt_scale_wind_turbine_rotor
29. Nazar W, Niedoszytko M. Air pollution in Poland: a 2022 narrative review with focus on respiratory diseases. Int J Environ Res Public Health. 2022 Jan 14;19(2):895.
30. Nazar W, Plata-Nazar K. Changes in air pollution-related behaviour measured by Google Trends search volume index in response to reported air quality in Poland. Int J Environ Res Public Health. 2021 Nov 8;18(21):11709.
31. Upadhyay A, Dey S, Chowdhury S, Goyal P. Expected health benefits from mitigation of emissions from major anthropogenic PM2.5 sources in India: statistics at state level. Environ Pollut 2018; 242: 1817–26.
32. Marmutovaa S. Grid convergence study of a Savonius wind turbine model. InProc. 27th Int. Conf. Effic. Cost, Optim. Simul. Environ. Impact Energy Syst. ECOS 2014.
33. Mohamed EA, Radhwi MN, Abdel Gawad AF. Computational investigation of aerodynamic characteristics and drag reduction of a bus model. American Journal of Aerospace Engineering. 2015;2(1-1):64-73.
34. Alonso-Estébanez, A., Del Coz Díaz, J. J., Álvarez Rabanal, F. P. & Pascual-Muñoz, P. (2017). Numerical simulation of bus aerodynamics on several classes of bridge decks. *Engineering Applications of Computational Fluid Mechanics*, *11*(1), 435-449. https://doi.org/10.1080/19942060.2016.1201544
35. Kim JJ, Baik JJ. A numerical study of the effects of ambient wind direction on flow and dispersion in urban street canyons using the RNG k–ε turbulence model. Atmospheric Environment. 2004 Jun 1;38(19):3039-48.
36. Bekhti A, Maizi M, Tata M, Laazab S. Numerical Investigation of Turbulent Flow over a Vertical axis Wind Turbine. In2019 7th International Renewable and Sustainable Energy Conference (IRSEC) 2019 Nov 27 (pp. 1-5). IEEE.
37. Bilgili M, Yasar A. Performance evaluation of a horizontal axis wind turbine in operation. International Journal of Green Energy. 2017 Sep 26;14(12):1048-56.
38. You JY, Yu DO, Kwon OJ. Effect of turbulence models on predicting HAWT rotor blade performances. Journal of Mechanical Science and Technology. 2013 Dec; 27:3703-11.

